International Journal of Power Electronics and Drive Systems (IJPEDS)
Vol. 12, No. 3, September 2021, pp. 1609~1619
ISSN: 2088-8694, DOI: 10.11591/ijpeds.v12.i3.pp1609-1619

Two-level inverter and three-level neutral point diode clamped inverter for traction applications: a comparative analysis study

Asmaa A. Abdelsalam[1], Mohamed Adel Esmaeel[2], Salama Abo Zaid[3]
[1]Tabbin Institute for Metallurgical Studies, Cairo, Egypt
[2]Department of Electrical Power and Machines Engineering, Faculty of Engineering, Helwan University, Cairo, Egypt
[2]Faculty of Engineering and Technology, Badr University in Cairo (BUC), Cairo, Egypt
[3]Department of Electrical Engineering, Faculty of Engineering, Al-Azhar University, Cairo, Egypt

Article Info

Article history:

Received Apr 21, 2021
Revised Jul 6, 2021
Accepted Jul 24, 2021

Keywords:

Conduction losses
Neutral point clamped inverter
Switching losses
Traction application
Transient response
Two-level inverter

ABSTRACT

This paper presents an analytical comparison between two-level inverter and three-level neutral point diode clamped inverters for electric vehicle traction purposes. The main objective of the research is to declare the main differences in the performance of the two inverter schemes in terms of the switching and conduction losses over an entire domain of the modulation index and the phase angle distribution, steady-state operation, transient operation at a wide range of speed variation, and the total harmonic distortion THD% of the line voltage output waveform. It also declares the analysis of the three-level neutral point diode clamped inverter (NPCI) obstacle and the unbalance of the DC-link capacitor voltages. The introduced scheme presents an Induction Motor (IM) drive for electric vehicle (EV) applications. Considering the dynamic operation of the EV, the speed of the three-phase induction motor is controlled using a scalar V/Hz control for the full range of the IM power factor (PF). A comprehensive MATLAB/Simulink model for the proposed scheme is established.

Corresponding Author:

Asmaa A. Abdelsalam
Tabbin Institute for Metallurgical Studies
11913 Tabbin, Helwan, Cairo, Egypt
Email: Asmaa.abdlsalam@gmail.com

1. INTRODUCTION

The motivation for the diminution of fuel consumption and harmful emissions in transportations increased the interest in developing the electrified power trains in the automotive industry, besides the advantages of low maintenance, cost-effectiveness, safety drive, popularity, and no noise pollution. Since breakdown is not accepted on the road, reliability is in high demand. Also, the allowed weight of the vehicle is a challengeable topic as mass production at low cost is a requirement. These matchless demands and trade-offs in traction applications pose significant challenges for the electrical propulsion system of EVs.

The EV propulsion system mainly consists of a motor, power inverter, and an educated control system. EV manufacturers majority utilize a two-level inverter for machine drives that is a well-established technique. Since the reduction of passive components in the traction drive, advanced control of the electric machine, and a rise of the inverter power density is a demand, the switching frequency increase of the converter to several kHz is a must. At high switching frequencies, two-level inverters have high power losses that reduce the inverter efficiency [1].

The recent direction for high power high voltage electric drives are multi-level inverters since they prove the production of an enhanced output voltage waveform, less total harmonic distortion (%THD), lower

switching losses at the high switching frequency, reduced electromagnetic interference (EMI) emission, and lower dv/dt [2]-[6]. The three-level Neutral Point Clamped Inverter (NPCI) has been introduced in 1981 by Akira Nabae and Isao Takahashi [7], then it has been taken into account in many medium and high-power industries. Above 6.5 kV, high voltage locomotives with high-speed, (NPCI) has found acceptance because of their various advantages like more minor switching losses, lower distortion, and the improved voltage waveform. Recently, many research papers mentioned that (NPCI) exhibits excellent accomplishment in terms of reliability, efficiency, and better frugal advantages, especially during high switching frequency operation. The switching losses of the NPCI are less than that for a two-level inverter for the same DC bus voltage as NPCI has a lower voltage rating for switches so when the switching frequency comes up, the switching losses go down [5], [8]. Hence, nowadays, manufacturers are directed to three-level NPCI for electric machine drives since it provides an increase of the dc voltage level despite the fact of its drawback; the capacitors' DC-link voltages unbalance.

For an EV, the most significant features of the electric motor are high reliability, low maintenance requirements, high efficiency, reliable drive control, besides the ability to handle voltage fluctuations of the source. Motors represented for EVs are Induction machines (IM), DC machines, permanent magnet synchronous machines (PMSMs), and switched reluctance machines (SRMs). Among the mentioned machines, the Induction motor has the advantages of elevated max. speed, a wide range of field weakening, higher power density, low no-load current, sturdy design, and low production costs. Nowadays, the semiconductors and power electronics uprising make the IM a strong candidate with better chances on the market for vehicle propulsion. Recently, multiple research has paid attention to an analytical comparison between two-level, Figure 1 (a), and three-level NPC inverters, Figure 1 (b) [1], [3], [5]. Several works of literature have mentioned the switching losses and harmonics comparisons however, steady-state and transient operation at different speeds is not discussed.

This research states a comparison between a two-level voltage source inverter and a three-level neutral point diode clamped inverter NPCI used for IM traction drives in terms of the switching losses, quality of the output voltage waveform, total harmonic distortion (THD%), steady-state and transient response taking into account the dynamic PF of the IM operation by MATLAB/Simulink. Figure 2 shows a simplified block diagram of the scheme.

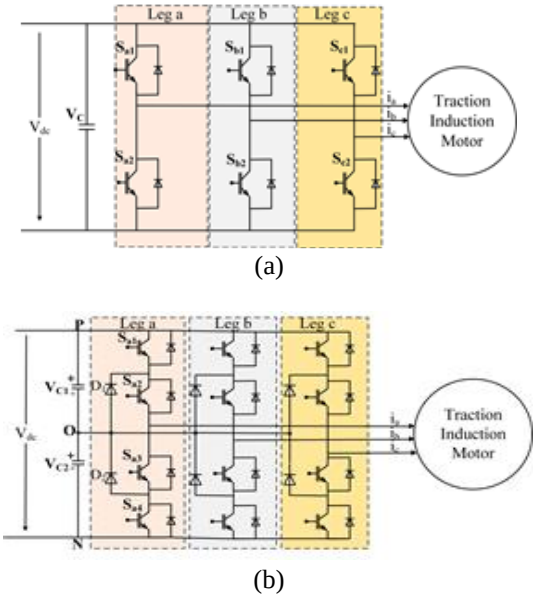

Figure 1. Two traction inverter schemes, (a) two-level voltage source inverter, (b) three-level neutral point clamped inverter

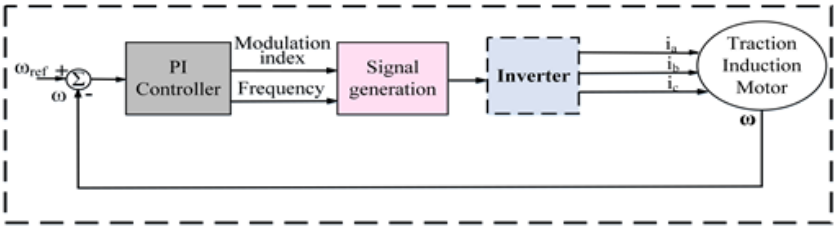

Figure 2. Simplified block diagram of the proposed scheme

The most popular pulse width modulation (PWM) techniques are multi-carrier sine pulse width modulation (SPWM) [9]-[11], Space Vector Pulse width Modulation (SVPWM) [12]-[16], and selective harmonic elimination PWM (SHE) [17]-[19]. The comparison between different techniques is made based on the output line voltage THD, the common-mode voltage, and the utilization of DC-link voltage [20], [21]. Figure 3 presents the classification of various PWM techniques. The most commonly used PWM control strategies are carrier-based PWM and space-vector-based PWM (SV-PWM) techniques due to the advanced PWM quality. In this work carrier-based, continuous PWM is applied to both Two-level and three-level inverters.

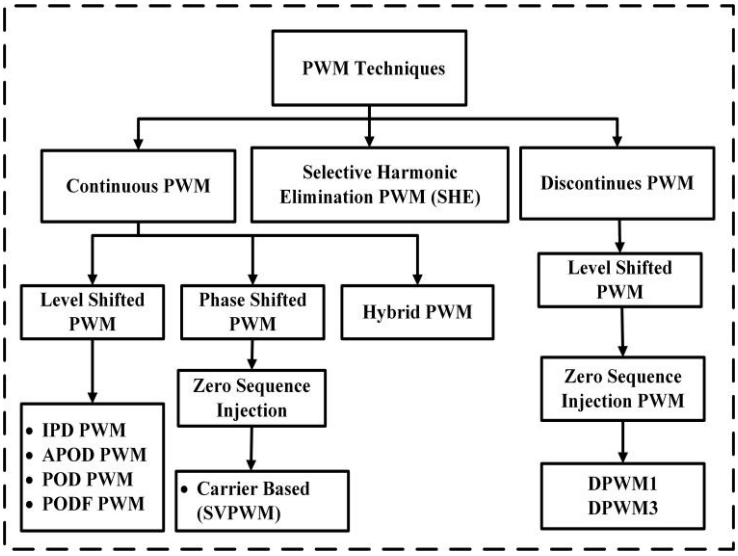

Figure 3. Various pulse width modulation topologies

2. OPERATING PRINCIPLE OF THREE-LEVEL NPCI

A Neutral point clamped three-phase inverter scheme is shown in Figure 1 (b). Each phase contains four IGBT switches and two clamping diodes (D_1 and D_2 for leg a), the midpoint of the two diodes is linked to the DC-link capacitors midpoint (O) [22]. Figure 4 illustrates phase/leg (a) as an example. Three statues of operation are shown. The neutral point (O) represents the zero-potential point.

First status, Figure 4 (a): the switches (S_{a1} and S_{a2}) are on, allowing the current i_{a1} to flow from the DC link to the load while switches (S_{a3} and S_{a4}) are off, the output voltage is $V_{dc}/2$. The current i_{a2} flows from the load to the DC power supply through the diodes of S_{a1} and S_{a2} that also provides an output voltage equal to $V_{dc}/2$. Second status, Figure 4 (b): the switches (S_{a2} and S_{a3}) are on, allowing the current i_{a1} to flow from the DC link to the load through D_1 and S_{a2} while switches ($S_{a1}$and S_{a4}) are off, producing an output voltage equal to zero. The current i_{a2} flows from the load to the DC power supply through D_2 and S_{a3} that also provides an output voltage equal to zero. Third status, Figure 4 (c): the switches (S_{a3} and S_{a4}) are on, allowing the current i_{a1} to flow from the DC link to the load through the clamping diodes of S_{a3} and S_{a4} while switches ($S_{a1}$and S_{a2}) are off, producing an output voltage equal to - $V_{dc}/2$. The current i_{a2} flows from the load to the DC power supply through S_{a3} and S_{a4} that also provides an output voltage equal to - $V_{dc}/2$.

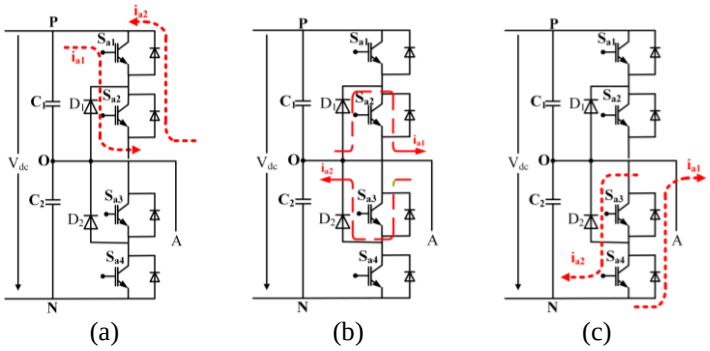

Figure 4. Three operation status of phase a: (a) first status, (b) second status, (c) third status

3. PERFORMANCE ANALYSIS

The performance evaluation of the introduced work is modeled by MATLAB/Simulink. A closed-loop scalar control V/Hz based induction motor drive is presented to obtain a transient response with different speeds, the quality of the waveform, the power loss analysis for both switching and conduction periods for full range distribution of the modulation index and load PF angle is introduced. The simulation parameters are: A DC-link voltage of 600 V for both two-level and three-level NPCI. The NPCI capacitors are 500 µF each, and the switching frequency is 5 kHz. The induction motor rating is 400 V, 5.4 HP, 4-pole, 50 Hz,1430 rpm, which is loaded by a dc-generator coupling.

3.1. Steady-state operation

This section inspects the steady-state performance of the applied scheme for both inverters. Figures 5 (a)-(d) and Figures 6 (a)-(d) demonstrate the waveform signals of the output line voltage, the electromagnetic torque, and the three-phase stator current at the rated speed of 1430 rpm of the two-level inverter and the three-level NPCI, respectively. It shows an almost sinusoidal output stator current for both inverters while the line voltage output quality of the NPCI is closer to the sinusoidal track waveform. The displayed results show acceptable behavior for the implemented scheme for the indicated speed and other speeds as well.

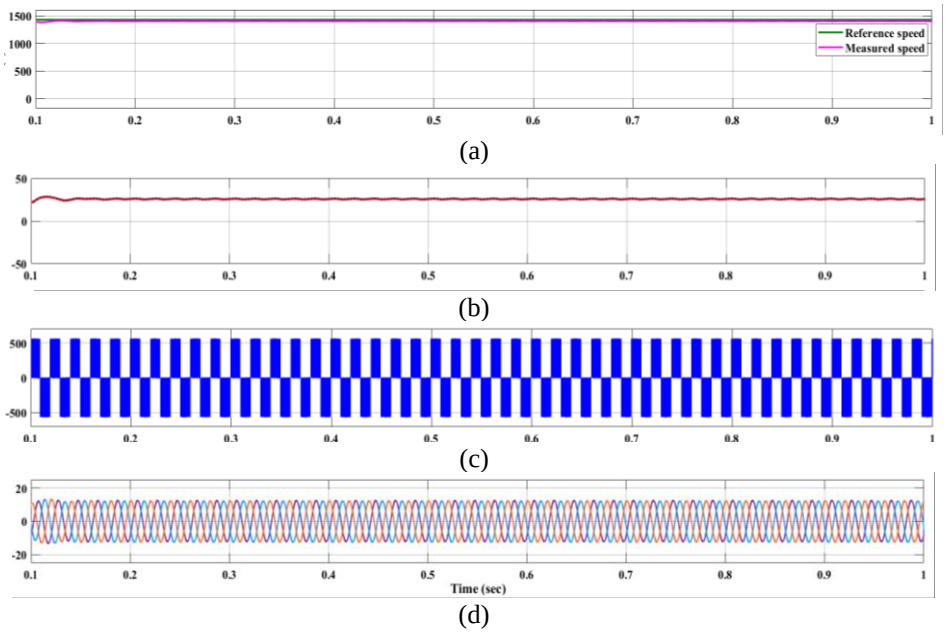

Figure 5. The simulation output waveforms of the two-level inverter at steady-state operation: (a) motor speed (rpm), (b) electromagnetic torque (N.m), (c) line voltage (V), and (d) 3 phase stator current (A)

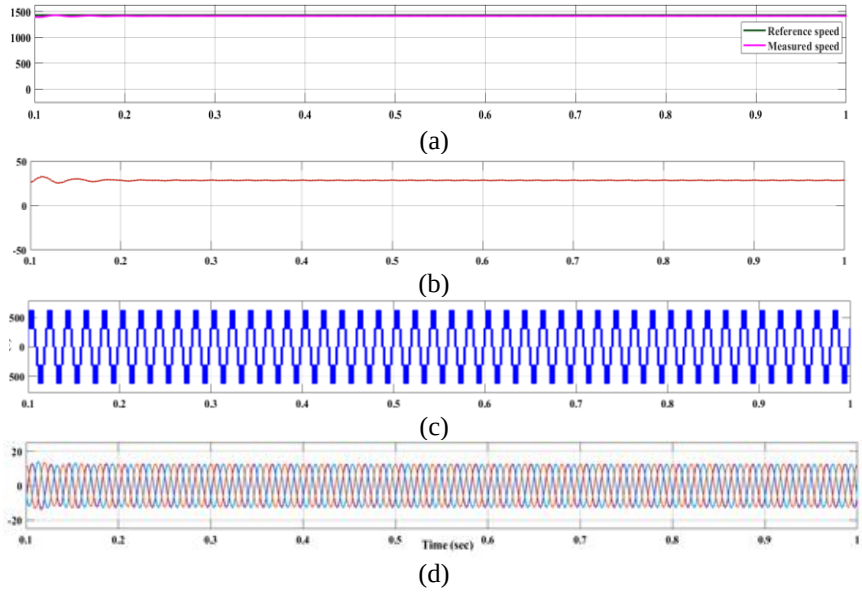

(a)

(b)

(c)

(d)

Figure 6. The simulation output waveforms of the NPCI at steady-state operation: (a) motor speed (rpm), (b) electromagnetic torque (N.m), (c) line voltage (V), and (d) 3 phase stator current (A)

3.2. Transient operation

The scheme attitude is examined during transients by changing the speed for the broad zone of operation. Figure 7(a)-(d), and Figure 8 (a)-(d), represent the performance for the two inverters for constant load torque of 27 N.m; while the speed varies, in the beginning, the induction motor operates with 500 rpm for 0.4 sec, then is raised to reach the rated speed, 1430 rpm for another 0.4 sec. Finally, the speed was declined to 1000 rpm. Figure 8 shows the transient performance of a three-level neutral point inverter over a range of different speeds. It is observed that the rise of the modulation index is meet by an increase of the output voltage steps to be closer to a sinusoidal wave-shape distribution if compared with the two-level inverter; as a result, the dv/dt stress across the power switches goes down. In Figure 8 (c), It is noticeable that the behavior of the line output voltage of the NPCI acts as that of the two-level inverter at 500 rpm due to the modulation technique used.

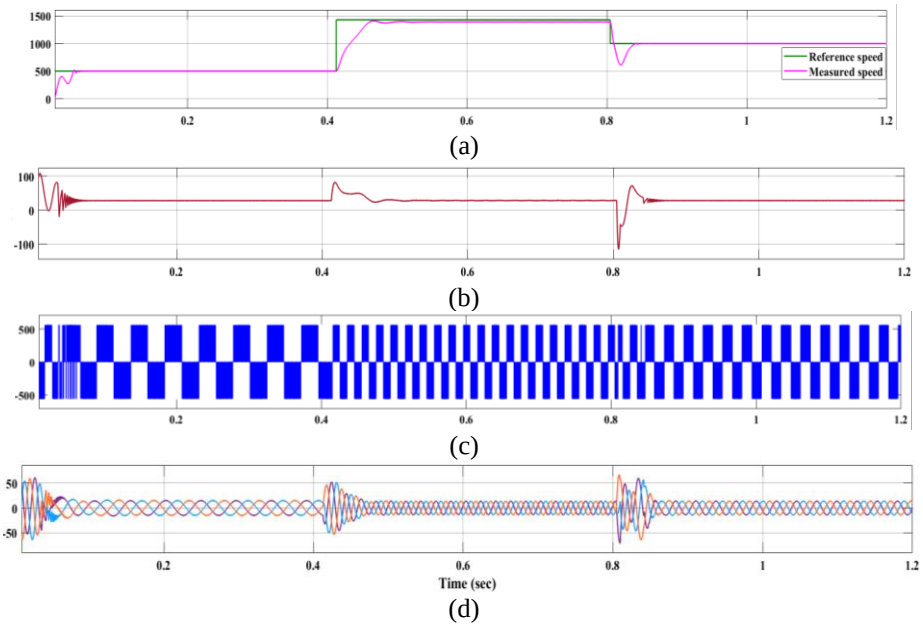

(a)

(b)

(c)

(d)

Figure 7. The simulation output waveforms of the two-level inverter at transient operation: (a) motor speed (rpm), (b) electromagnetic torque (N.m), (c) line voltage (V), and (d) 3 phase stator current (A)

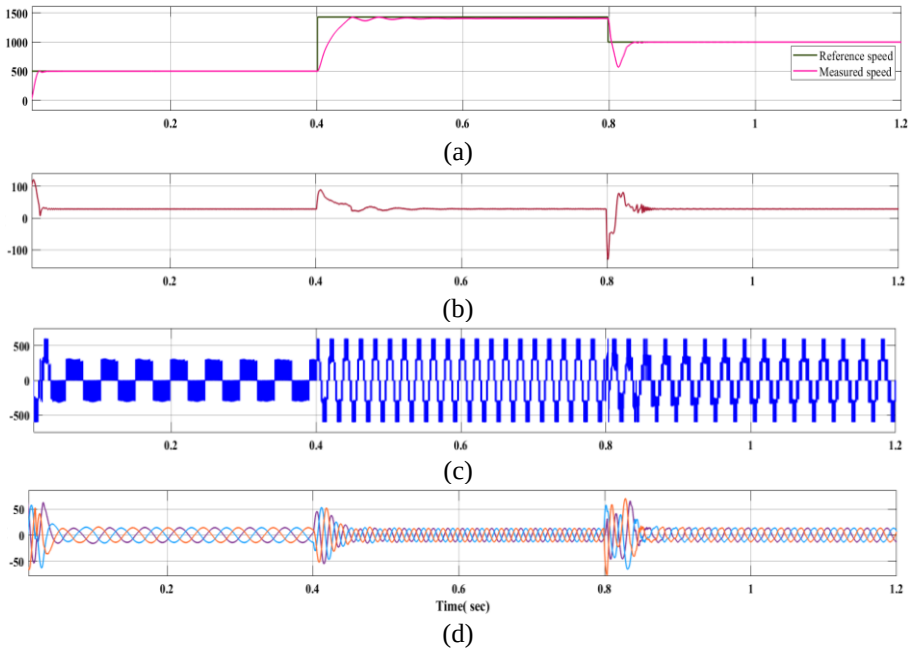

(a) (b) (c) (d)

Figure 8. The simulation output waveforms of the NPCI at transient operation: (a) motor speed (rpm), (b) electromagnetic torque (N.m), (c) line voltage (V), and (d) 3 phase stator current (A)

4. CONDUCTION POWER LOSS CALCULATIONS

4.1. Two-level inverter

The two-level inverter conduction losses have been investigated for the inverter switches, IGBT and its anti-parallel diode over a full range distribution of the modulation index (m) ($0 < m < 1$) and a full range of the phase angle (φ) ($0 < \varphi < \pi/2$). The conduction losses of a single IGBT switch and its anti-parallel diode could be described as given in (1) and (2), respectively [2]:

$$p_{cs} = (V_{cs}.I_m).(\frac{1}{2\pi} + \frac{0.7853}{2\pi}.m.cos(\phi)) \quad (1)$$

$$p_{cd} = (V_{cd}.I_m).(\frac{1}{2\pi} - \frac{0.7853}{2\pi}.m.cos(\phi)) \quad (2)$$

Where P_{cs} is the average conduction losses in power switches and P_{cd} is the average conduction losses in the anti-parallel diodes. V_{cd} is the saturation voltage of the anti-parallel diodes while V_{cs} is the saturation voltage of the IGBT switch. The maximum phase peak current is denoted as I_m.

Figure 9 shows the conduction losses of the two-level inverter at different modulation indexes and different phase angles. The IGBT losses are shown in Figure 9 (a), while the ani-parallel diode losses are depicted in Figure 9 (b). It is evident that with the modulation index rise, the conduction losses of the IGBT come up while the opposite acquires with their anti-parallel diodes; the conduction losses decrease with the modulation index increase. In contrast, the rise in the power factor angle reduces the IGBT conduction losses and shift up the anti-parallel diode losses.

4.2. Three-level NPCI

For a 3-level NPCI, the IGBT switches S_{a1} and S_{a4} have the same conduction period; thus, both switches have the same conduction losses $P_c)_{S_{a1},S_{a4}}$. Similarly, with switches S_{a2} and S_{a3}. The average IGBT switches conduction losses $P_c)_{S_{a2},S_{a3}}$ are expressed in (3) and (4) [2]:

$$P_c)_{S_{a1},S_{a4}} = (\frac{V_{cs}.I_m.m}{4\pi}).((\pi - \varphi).cos(\varphi) + sin(\varphi)) \quad (3)$$

$$P_c)_{S_{a2},S_{a3}} = (\frac{V_{cs}.I_m}{\pi}).(\frac{V_{cs}.I_m.m}{4\pi}.(\varphi.cos(\varphi) - sin(\varphi))) \quad (4)$$

While the conduction losses of the clamping diodes D_1 and D_2, $P_c)_{D_1,D_2}$ are given in (5) and for the anti-parallel diodes D_a, $P_{c_{D_a}}$ in (6).

$$P_c)_{D_1,D_2} = (\frac{V_{cs}.I_m.m}{4\pi}).(4 + m.(2\varphi - \pi).cos(\varphi) - 2\,sin(\varphi)) \quad (5)$$

$$P_{c_{D_a}} = (\frac{V_{cD}.I_m.m}{4\pi}).(sin(\varphi) - \varphi\,cos(\varphi)) \quad (6)$$

Figures 10 (a) and 10 (b) describes the role of the modulation index and the phase angle variation on the IGBT switches' conduction loss. While the conduction losses of the NPCI clamping and anti-parallel diodes are presented in Figures 10 (c) and 10 (d), respectively. The rise of the modulation index is met by an increase in the conduction loss while it declines with the increment of the power factor angle. Unlike the two-level inverter, Figure 9, the 3-level NPCI switches do not have equal conduction power losses distribution, which leads to inhomogeneous heat distribution over the different switches. The anti-parallel diode of the NPCI IGBT switch has almost half of the maximum conduction loss of the two-level inverter's one.

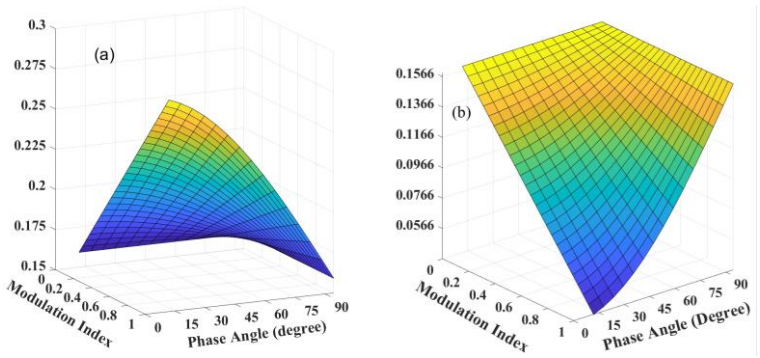

Figure 9. The two-level inverter conduction losses at different modulation index and different phase angles, (a) IGBT losses, (b) anti-parallel diode losses

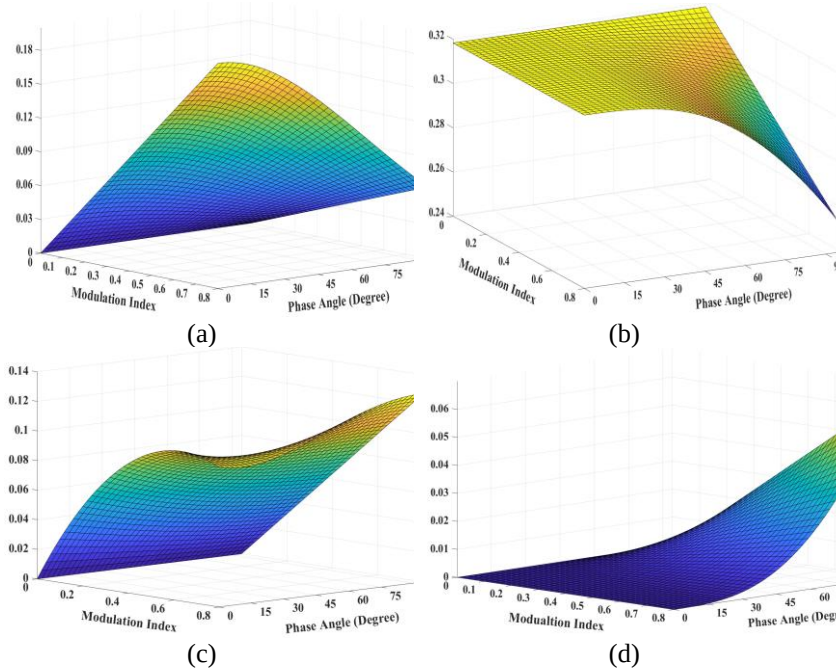

Figure 10. The conduction losses of NPCI at different modulation index and different phase angles, (a) S_{a1}, S_{a4}, (b) S_{a2}, S_{a3}, (c) clamping diodes D_1 and D_2, and (d) anti-parallel diodes

5. SWITCHING POWER LOSS CALCULATIONS

5.1. Two-level inverter

The voltage across the switch and the load current are defining its power-switching losses. Turn-on "Eon "and turn-off "Eoff" losses are the observed loss for an IGBT. Commonly both of them are defined by the manufacturer. The diode has only reverse recovery losses during turn-off periods Err. Hence the average switching losses for an IGBT is P_{ss} and for the anti-parallel diode is P_{sd} can be expressed as in (7) and (8) where the datasheet nominal voltage for IGBT losses is V_{nom} and the switching frequency is f_{sw} [2]:

$$P_{ss} = (\frac{1}{2\pi}) \int_{\varphi}^{\pi+\varphi} ((E_{on} + E_{off}).(\frac{V_{cs}}{V_{nom}}).f_{sw})\, d\omega t \quad (7)$$

$$P_{sd} = (\frac{1}{2\pi}) \int_{\varphi}^{\pi+\varphi} (E_{rr}.(\frac{V_{cs}}{V_{nom}}).f_{sw})\, d\omega t \quad (8)$$

Considering $E = E_{on} + E_{off}$ is the total switching losses as a function of the load current, the E_{IGBT} and E_{Diode} can be expressed as shown in (9) and (10):

$$E_{IGBT} = -2e^{-7}.i^2 + 2e^{-4}.i + 4e^{-4} \quad (9)$$

$$E_{Diode} = -9e^{-8}.i^2 + 8e^{-5}.i + 6e^{-3} \quad (10)$$

Replacing the values of the switching losses from (9) and (10) into (7) and (8), yields:

$$P_{ss} = (\frac{1}{2\pi}).(-1.1413\, e^{-7}.{I_m}^2 + 2\, e^{-4}.I_m + 0.00125).(\frac{V_{cs}}{V_{nom}}).f_{sw} \quad (11)$$

$$P_{sd} = (\frac{1}{2\pi}).(-1.1413\, e^{-7}.{I_m}^2 + 1.6\, e^{-4}.I_m + 0.0188).(\frac{V_{cs}}{V_{nom}}).f_{sw} \quad (12)$$

From the (11) and (12), it is perspicuous that the switching losses are mainly related to the switching frequency. The losses are directly proportional to the switching frequency, and it does not depend on the modulation index.

5.2. Three-level inverter

The average switching power losses P_{sw} of the NPCI switches can be calculated as [2]:

$$P_{swS_{a1}} = P_{swS_{a4}} = (\frac{1}{2\pi}).(I_m^2.(5e^{-9}\varphi - 1.57\, e^{-8} - 25\, e^{-10}.sin(2\varphi)) + 6\, e^{-5}.I_m(1 + cos(\varphi)) - 31\, e^{-4}.\varphi + 0.00973).(\frac{V_{Cs}}{V_{nom}}).f_{sw} \quad (13)$$

$$P_{swS_{a2}} = P_{swS_{a3}} = \left(\frac{1}{2\pi}\right).(I_m^2.(25\, e^{-10}\, sin(2\varphi) - 5e^{-9}\varphi) + 6\, e^{-5}.I_m(1 - cos(\varphi)) + 31\, e^{-4}.\varphi).(\frac{V_{Cs}}{V_{nom}}).f_{sw} \quad (14)$$

$$P_{swD_a} = (\frac{1}{2\pi}).(I_m^2.(75\, e^{-10}.sin(2\phi) - 15\, e^{-9}\phi) + 3\, e^{-5}.I_m(cos(\phi) - 1) - 11\, e^{-4}.\phi).(\frac{V_{Cs}}{V_{nom}}).f_{sw} \quad (15)$$

$$P_{swD_1} = P_{swD_2} = (\frac{1}{2\pi}).(6\, e^{-5}.I_m - 4.71\, e^{-8}.I_m^2 + 0.0034).(\frac{V_{Cs}}{V_{nom}}).f_{sw} \quad (16)$$

From expressions, it is clear that the four IGBT switches for the three-level NPC inverter have the same switching power loss distribution, same for the anti-parallel diodes and the two clamped diodes. The switching losses depend on the switching frequency and do not rely on the modulation index. Since the number of switches/leg is greater than that of the two-level inverter then the NPCI switching losses for the single switch are lower.

6. THE THREE-LEVEL NPCI CAPACITOR VOLTAGES UNBALANCE

In an EV that runs with an NPCI induction motor drive, a periodic dc-link voltage unbalance may exist due to the dynamic operating conditions. The major reason for this unbalance is the flow of average

current in the neutral point because of the unregular switching of the nonideal components; the modulation topology applied is also a reason. This non-zero neutral current generates accelerated fluctuations that cause the voltage two unbalance the two dc-link capacitors. For steady, reliable operation of an NPCI, these voltage fluctuations, shown in Figure 11 are unwanted for balanced EV traction inverter drive. The modulation technique applied should be able to reduce this unbalance issue in case no external circuit is added. Many researchers have reported solutions for the unbalance of the neutral current [23]–[26]. In [26], the neutral point current was reduced by adding a measured zero-sequence voltage signal to the reference voltages, which improved the converter performance that is highly recommended for EVs applications.

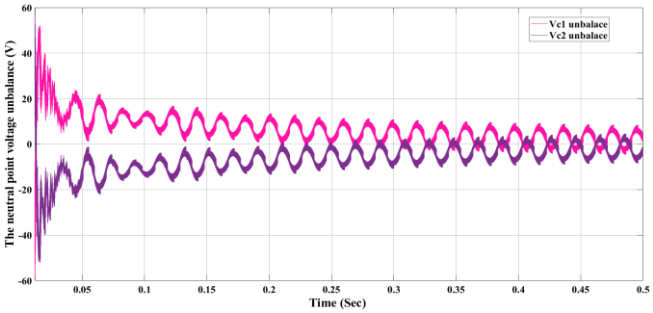

Figure 11. The NPCI capacitors voltage unbalance

7. TOTAL HARMONIC DISTORTION (THD%)

The output line voltage THD% of the two-level inverter is illustrated in Figure 12 (a) while, the NPCI output voltage THD% is presented in Figure 12 (b). Form Figure 12 (a) and Figure 12 (b), it is obvious that the NPC 3-level inverter THD% is almost 50% less than that of the two-level inverter at the same modulation index. The THD% remarkable reduction leads to the deduction of the size of the passive components such as the inductor of the interference filter on the load side and the electromagnetic filter that existed at the source side, which leads to the reduction of the system power losses existed at the source side.

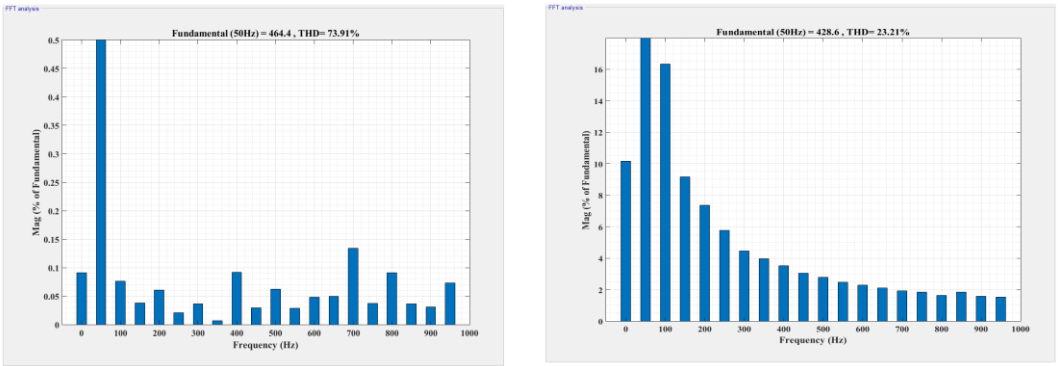

(a) (b)

Figure 12. THD% of, (a) two-level inverter, (b) three-level NPCI

8. CONCLUSION

This paper compares the operation of a two-level inverter and a three-level NPCI traction IM drive using MATLAB/Simulink. The comparative performance analysis has been classified into different attributes, which are the steady-state operation, the transient operation at a wide range of speed variation, the power loss, including both conduction and switching losses calculations for a full range of modulation index distribution and PF angle variation, waveform quality, and the total harmonic distortion of the output line voltage for both inverters. Also, the dc-link capacitors' unbalance voltage of the NPCI is analyzed. The output results of the applied scheme show its applicability with both inverter drives. The total harmonic distortion of the NPCI output line voltage is 50% lower than that for the two-level inverter at the same

modulation index using the control topology introduced. Hence, Using the three-level neutral point diode clamped as an induction motor drive-based Electric Vehicle is considered an attractive candidate.

REFERENCES

[1] A. Choudhury, P. Pillay, and S. S. Williamson, "Comparative analysis between two-level and three-level DC/AC electric vehicle traction inverters using a novel DC-link voltage balancing algorithm," *IEEE Journal of Emerging and Selected Topics in Power Electronics*, vol. 2, no. 3, pp. 529-540, 2014, doi: 10.1109/jestpe.2014.2310140.

[2] A. Choudhury, "Three-level neutral point clamped (NPC) traction inverter drive for electric vehicles," Ph.D Dissertation, Department of Electrical and Computer Engineering Concordia University, Montreal, 2015.

[3] M. Schweizer, T. Friedli, and J. W. Kolar, "Comparative evaluation of advanced three-phase three-level inverter/converter topologies against two-level systems," *IEEE Transactions on Industrial Electronics.*, vol. 60, no. 12, pp. 5515-5527, 2013, doi: 10.1109/TIE.2012.2233698.

[4] S. De, D. Banerjee, K. Siva Kumar, K. Gopakumar, R. Ramchand, and C. Patel, "Multi-level inverters for low-power application," *IET Power Electronics*, vol. 4, no. 4, pp. 384-392, Apr. 2011, doi: 10.1049/iet-pel.2010.0027.

[5] R. Teichmann and S. Bernet, "A comparison of three-level converters versus two-level converters for low-voltage drives, traction, and utility applications," *IEEE Transactions on Industry Applications*, vol. 41, no. 3, pp. 855-865, May 2005, doi: 10.1109/TIA.2005.847285.

[6] B. A. Welchko, M. B. De Rossiter Correa, and T. A. Lipo, "A three-level MOSFET inverter for low-power drives," *IEEE Transactions on Industry Applications*, vol. 51, no. 3, pp. 669-674, Jun. 2004, doi: 10.1109/TIE.2004.825337.

[7] A. Nabae, I. Takahashi, and H. Akagi, "A new neutral-point-clamped PWM inverter," *IEEE Transactions on Industry Applications*, vol. IA-17, no. 5, pp. 518-523, 1981, doi: 10.1109/TIA.1981.4503992.

[8] S. M. Sharkh, M. A. Abusara, G. I. Orfanoudakis, and B. Hussain, "Loss comparison of two- and three-level inverter topologies," in *Power Electronic Converters for Microgrids*, John Wiley & Sons, Singapore Pte. Ltd, 2014, pp. 51-72. doi:10.1002/9780470824054.

[9] J. Pou, J. Zaragoza, S. Ceballos, M. Saeedifard, and D. Boroyevich, "A carrier-based PWM strategy with zero-sequence voltage injection for a three-level neutral-point-clamped converter," *IEEE Transactions on Power Electronics*, vol. 27, no. 2, pp. 642-651, 2012, doi: 10.1109/TPEL.2010.2050783.

[10] J. H. Kim, S. K. Sul, and P. N. Enjeti, "A carrier-based PWM method with optimal switching sequence for a multi-level four-leg voltage-source inverter," *IEEE Transactions on Industry Applications*, vol. 44, no. 4, pp. 1239-1248, 2008, doi: 10.1109/TIA.2008.926201.

[11] D. G. Holmes and T. A. Lipo, *Pulse width modulation for power converters principles and practice*, New Jersey: Wiley-IEEE Press, 2003.

[12] A. R. Beig, "Synchronized SVPWM algorithm for the overmodulation region of a low switching frequency medium-voltage three-level VSI," *IEEE Transactions on Industrial Electronics*, vol. 59, no. 12, pp. 4545-4554, 2012, doi: 10.1109/TIE.2011.2182016.

[13] S. Das and G. Narayanan, "Novel switching sequences for a space-vector-modulated three-level inverter," *IEEE Transactions on Industrial Electronics*, vol. 59, no. 3, pp. 1477-1487, Mar. 2012, doi: 10.1109/TIE.2011.2163373.

[14] M. C. Cavalcanti, A. M. Farias, K. C. Oliveira, F. A. S. Neves, and J. L. Afonso, "Eliminating leakage currents in neutral point clamped inverters for photovoltaic systems," *IEEE Transactions on Industrial Electronics*, vol. 59, no. 1, pp. 435-443, Jan. 2012, doi: 10.1109/TIE.2011.2138671.

[15] T. Ghennam, E. M. Berkouk, and B. Francois, "A novel space-vector current control based on circular hysteresis areas of a three-phase neutral-point-clamped inverter," *IEEE Transactions on Industrial Electronics*, vol. 57, no. 8, pp. 2669-2678, 2010, doi: 10.1109/TIE.2009.2035458.

[16] A. Mehrizi-Sani, and S. Filizadeh, "An optimized space vector modulation sequence for improved harmonic performance," *IEEE Transactions on Industrial Electronics*, vol. 56, no. 8, pp. 2894-2903, 2009, doi: 10.1109/TIE.2008.2008997.

[17] Y. Zhang, Z. Zhao, and J. Zhu, "A hybrid PWM applied to high-power three-level inverter-fed induction-motor drives," *IEEE Transactions on Industrial Electronics*, vol. 58, no. 8, pp. 3409-3420, Aug. 2011, doi: 10.1109/TIE.2010.2090836.

[18] J. Napoles, J. I. Leon, R. Portillo, L. G. Franquelo, and M. A. Aguirre, "Selective harmonic mitigation technique for high-power converters," *IEEE Transactions on Industrial Electronics*, vol. 57, no. 7, pp. 2315-2323, Jul. 2010, doi: 10.1109/TIE.2009.2026759.

[19] S. Sirisukprasert, J. S. Lai, and T. H. Liu, "Optimum harmonic reduction with a wide range of modulation indexes for multi-level converters," *IEEE Transactions on Industrial Electronics*, vol. 49, no. 4, pp. 875-881, Aug. 2002, doi: 10.1109/TIE.2002.801226.

[20] G. J. Rushiraj and P. N. Kapil, "Analysis of different modulation techniques for multi-level inverters," in *International Conference on Electrical, Electronics, and Optimization Techniques, ICEEOT 2016*, Nov. 2016, pp. 3017-3022, doi: 10.1109/ICEEOT.2016.7755254.

[21] M. Sajitha, J. Sandeep, and R. Ramchand, "Comparative analysis of different modulation techniques for three level three phase T-type NPC inverter," in *IEEE Region 10 Annual International Conference, Proceedings/TENCON*, Oct. 2019, vol. 2019-Octob, pp. 1529-1534, doi: 10.1109/TENCON.2019.8929574.

[22] Q. Yuan, J. Qian, and A. Li, "A simplified common-mode voltage suppression and neutral-point potential control for the NPC three-level inverter," *J. Electr. Eng. Technol.*, vol. 14, no. 6, pp. 2389-2398, 2019, doi: 10.1007/s42835-019-00293-9.

[23] F. Umbría, F. Gordillo, F. Gómez-Estern, F. Salas, R. C. Portillo, and S. Vázquez, "Voltage balancing in three-level neutral-point-clamped converters via Luenberger observer," C*ontrol Eng. Pract*., vol. 25, no. 1, pp. 36-44, 2014. doi:10.1016/j.conengprac.2013.12.003.
[24] J. Pou, R. Pindado, D. Boroyevich, and P. Rodríguez, "Evaluation of the low-frequency neutral-point voltage oscillations in the three-level inverter," *IEEE Transactions on Industrial Electronics*, vol. 52, no. 6, pp. 1582-1588, Dec. 2005, doi: 10.1109/TIE.2005.858723.
[25] R. Krishna, D. E. Soman, S. K. Kottayil, and M. Leijon, "Synchronous current compensator for a self-balanced three-level neutral point clamped inverter," *Adv. Power Electron.*, vol. 2014, 2014, doi: 10.1155/2014/620607.
[26] I. López *et al.*, "Generalized PWM-based method for multiphase neutral-point-clamped converters with capacitor voltage balance capability." *IEEE Transactions on Power Electronics*, vol. 32, no. 6, pp. 4878-4890, 2017. doi**:** 10.1109/TPEL.2016.2599872.

BIOGRAPHIES OF AUTHORS

Asmaa A. Abdelsalam received a B.Sc. from the Faculty of Engineering, Helwan University. She works as an Electrical Engineer at Tabbin Institute for Metallurgical Studies, Cairo, Egypt. Currently, she is pursuing her master's degree in Electrical Engineering at the faculty of Engineering, Al-Azhar University. Her research interests include renewable energy, electrical machines, power electronics, photovoltaic, energy-storage applications, and space power applications.

Mohamed Adel Esmaeel Salama received the B.Sc., M.Sc. .and Ph.D. in 2004, 2009, and 2012 respectively from Helwan University and Al-Azhar University. He works as a lecturer for the Faculty of Engineering and Technology, Helwan University, and Delegated Badr University in Cairo (BUC), Cairo, Egypt. His research interests include renewable energy, electrical machines, power electronics, photovoltaic, energy-storage applications, and space power applications.

Salama Abu-Zaid is an associated Professor, Head of the Department of Electrical Power and Machine, Faculty of Engineering, Al Azhar University, Cairo, Egypt.